



HAL
open science

Integrating Thermal Properties and Degradation Modelling of Batteries into the Scheduling of Hybrid Power Plants with Photovoltaics

Alberto Vazquez-Rodriguez, Andrea Michiorri, Georges Kariniotakis

► **To cite this version:**

Alberto Vazquez-Rodriguez, Andrea Michiorri, Georges Kariniotakis. Integrating Thermal Properties and Degradation Modelling of Batteries into the Scheduling of Hybrid Power Plants with Photovoltaics. Journal of Energy Storage, 2023, 73 (Part A), pp.108782. 10.1016/j.est.2023.108782 . hal-04192269

HAL Id: hal-04192269

<https://hal.science/hal-04192269>

Submitted on 12 Sep 2023

HAL is a multi-disciplinary open access archive for the deposit and dissemination of scientific research documents, whether they are published or not. The documents may come from teaching and research institutions in France or abroad, or from public or private research centers.

L'archive ouverte pluridisciplinaire **HAL**, est destinée au dépôt et à la diffusion de documents scientifiques de niveau recherche, publiés ou non, émanant des établissements d'enseignement et de recherche français ou étrangers, des laboratoires publics ou privés.

Integrating Thermal Properties and Degradation Modelling of Batteries into the Scheduling of Hybrid Power Plants with Photovoltaics

Alberto Vazquez-Rodriguez^{a,b,*}, Andrea Michiorri^a, Georges Kariniotakis^a

^a*MINES Paris, PSL University, Centre PERSEE, Sophia-Antipolis France*

^b*SPIE Industrie, Aix-en-Provence, France*

Abstract

Renewable energy penetration in the energy mix has risen sharply in the last decade, and brought with it an increased deployment of large-capacity storage systems. The result is a need for optimised management strategies that integrate and safely operate the whole energy production chain, including precise models for each element that they control. This paper presents the results of a study on detailed state-of-charge, thermal and degradation modelling of Battery Energy Storage Systems for hybrid photovoltaic-battery power plants. The objective is to quantify the error associated with not taking into account a precise model for these parameters in industrial applications. The use case of optimal battery scheduling in a capacity firming framework and a low-voltage grid is considered to quantify the impact of these models. The proposed models for these parameters were developed and then validated against experimental measures from five hybrid power plants. The models were then applied to calculate optimal battery schedules, and showed lower than expected state-of-health loss values. The impact of including the thermal modelling in the scheduling process was also observed to be weaker than expected.

Keywords: Battery energy storage, Thermal modelling, State of health, Degradation, Optimal scheduling, Capacity firming, Hybrid PV-battery plant

*Corresponding author

Email address: aevazquezr@gmail.com (Alberto Vazquez-Rodriguez)

Nomenclature			
λ^j	Convection heat exchange coefficient.	$P_i^{k_0 \rightarrow k_1}$	Power from resource k_0 to k_1 , where $\{k_0, k_1\} \in k$.
B	Storage/Battery resource, the aggregation of all batteries j .	P_i^k	Power output from the energy resource k .
C_p^j	Thermal capacity.	P_{max}^k	Maximal power output from the energy resource k .
c_k	Cost associated with each energy source k .	P_{min}^k	Minimal power output from the energy resource k .
E_0^j	Initial energy capacity.	$P_{i,in}^S$	Solar power available.
G	Electrical grid.	R_{int}^j	Internal resistance.
i	Time instant i .	S	Solar resource.
j	Unique battery identifier.	S^*	Unexploited solar resource.
k	Energy resource, where $k = G, S, S^*, B, j$.	T_i^j	Internal temperature.
L_i	Local load.	T_{air}	Ambient air temperature.

1. Introduction

Battery Energy Storage Systems (BESS) represent a key factor to increase weather-dependent variable Renewable Energy Sources (vRES) penetration in the energy mix. The associated costs of the capacity reserve requirements to meet peak loads and maintain grid stability for such scenarios have been widely discussed over the years [1–4]. At the same time, continuous technological advances on lithium-based BESS and a nearly 90% price decrease since 2010 [5] have propelled grid-scale storage integration [6–8].

Lithium-ion (Li-ion) BESS are particularly interesting for vRES applications thanks to their fast dynamic response, high energy density, high efficiency and durability [9], which makes them a potential asset in new markets using demand-response mechanisms, capacity firming frameworks

and/or providing ancillary services [10, 11]. Schmidt et al. showed how li-ion BESS could become the most flexible and cost-effective storage technology in a 10-year horizon [12], and it is expected that at least a total of 16 GWh will be installed by the end of 2050 in the US market alone[13].

It is this expansion into different applications and markets, particularly for high capacity usages, that increases the need for a better understanding of BESS and the behaviour of their components. Li-ion BESS are particularly sensitive to thermal-related degradation, as operation in certain ranges of temperature can impact the power output, capacity, self-discharge rate, and the probability of thermal leakage [14, 15]. To reduce the occurrence of these phenomena, Battery Management Systems (BMS) are implemented to estimate the state of charge (SoC) and state of health (SoH), and to control the BESS operation [16]. Different BMS approaches, either at cell, module or system level, are used depending on the application[17], and new electrical and control architectures are constantly being developed to improve BESS performance and accuracy [18–20].

Regarding the numerical model used internally by BMS, several approaches and techniques exist. Electrochemical and physical models are primarily based on the Doyle-Fuller-Newman (DFN). Multiple approaches have been reported in the literature [21] as these models often offer very high accuracy, but their computational cost is high [21–24] and their implementation into embedded solutions has been limited although it is slowly increasing [25–27]. Equivalent circuit models (ECM) [28, 29] and machine learning (ML) models with state estimation algorithms [30–32] are more commonly used as they offer faster implementation and lower computing requirements.

Another challenge that arises from BESS integration in new domains is the unknown response the system can have in the short and long terms under the load profiles and operation conditions [33]. The ensemble of advances in BMS has allowed distributed systems operators (DSO) and vRES investors to incorporate BESS under different grid-scale scenarios including storage devices aggregation; however, the safety, optimal operation and profitability of such systems over the lifespan of projects are ongoing subjects of interest [34–38]. While multiple methods and objectives exist to achieve optimal BESS operation for vRES systems, financial targets are generally expressed in standard optimisation forms that are solved by search-based mathematical solvers[39].

The analysis of the literature above shows that, although data related to laboratory experiments on battery cell degradation are available, there is

a lack of information about the actual behaviour of BESS in real operating conditions. This makes it difficult to understand the impact of the thermal component of the SoC estimation and the degradation of long-term battery operation.

In this work, we present the development and impact of BESS state-of-charge and temperature models on the operation of hybrid power plants composed of a BESS system and a photovoltaic plant. The two operational use cases of interest are: a PV capacity firming framework, which traditionally receives less attention in the literature but which is essential in vulnerable grids to increase the integration of large-scale PV systems [40, 41]; and a battery aggregation scenario, a common target of battery energy management systems [39]. In both, energy availability and expected revenues are considered as a result of the optimal short-term scheduling process in the light of the used BESS models. In previous research, the capacity firming scenario has seen the application of stochastic and deterministic strategies which aim to propose a solution to the PV uncertainty [40, 42, 43], but not the behaviour of the BESS. The objective here is to showcase the importance of integrating advanced BESS models in short- and long-term revenue projections for new hybrid vRES projects.

First, we recovered long series of measurements issued from operational PV-BESS hybrid plants under a specific PV capacity firming framework. The nature of these data is highly dependent on the different equipment manufacturers as well as the SCADA on site. Using the collected measurements, a temperature predictor model was built and validated using the power profile and recorded temperatures. A SoC model based on a power counter was also parameterised, and an explicit integration of the battery temperature was taken into account. Lastly, a SoH model was trained based on the total throughput energy from the BESS.

The output predictions of the different battery models were then evaluated and afterwards incorporated in two optimisation frameworks: the first follows a specific PV capacity firming objective, and the second framework aims to reduce the unmet load in a nodal point composed of several network-attached storage systems and an RES plant, in this case a PV solar plant. The resulting power profiles were then used to evaluate the expected battery degradation, the financial profits, and the levelised cost of energy (LCOE) while complying with the grid requirements. In these results, explicit interest was given to the estimated internal temperatures, which are traditionally ignored in such optimisation frameworks.

In light of this, we can summarise the following three key contributions provided by this paper:

- We provide experimental results on thermal behaviour and degradation from several operational MW- grid-scale BESS under capacity firming constraints. This contrasts with many studies in the literature that are based on laboratory data on small-scale batteries.
- We define a framework of SoC, thermal and SoH models that are compatible with the data scarcity of industrial sites. Again, this is in contrast with most of the existing literature, which focuses on maximising models' accuracy in the presence of rich data sources.
- We assess how temperature and degradation consideration impacts scheduling with and without flexibility requirements. As a result, we can link the specific models to the value obtained at the end of the model chain. Such inclusions have not been widely discussed in previous related studies.

This paper is structured as follows: after the introduction presented in Section 1 above, the modelling is divided into two parts: models concerning thermal behaviour and SoH degradation are presented in Section 2, with a Section 2.1 establishing the data constraints imposed by industrial sites, while the modelling for the two optimal scheduling scenarios used for the evaluation are presented in Sections 3 and 4. Finally, the results are presented in Section 5 and conclusions are drawn in Section 6.

2. Battery Modelling

2.1. Observability of industrial BESS systems

This work focuses on industrial and grid-scale hybrid PV plants, and for this reason we consider the limits and constraints featured in such installations. One particular constraint is the scarcity of in-depth operational data from BESS and PV systems. In general, to maintain low costs and to avoid warranty disputes due to equipment alteration, only the minimum required sensors are installed, and most of the measurements come directly through the different equipment communication interfaces. As a consequence, the types of measurement available depend on the equipment and the data disclosure policy of the manufacturer. While efforts have been made to standardise the published data per kind of equipment [44, 45], manufacturers are

not required to apply the standards nor to make all of the internally measured information available to the client, except for compulsory details when adopting the standards. Furthermore, diagnostic procedures in both PV and storage systems are not common due to the loss of revenue involved, and thus the operational range of the data is restricted to the standard behaviour on site.

As such, only a limited amount of measured variables can be considered to be constantly available independently from the equipment installed. For solar inverters, these typically include the AC power measurements and meteorological data (irradiation and ambient temperature), with the BESS inverter offering in addition a state-of-charge (or equivalent) value. However, the state-of-health, DC and temperature measurements from the BESS cannot be considered as always available. A general approach to industrial in-situ BESS modelling must take into account these data availability limitations, and primarily use the measurements that are or will be accessible from the deployed system.

The models presented in the next sections reflect this application scenario.

2.2. Modelling battery temperature behaviour

When internal battery temperature measurements are available, the thermal dynamic behaviour of the BESS can be modelled using the standard heat equation in (1), in which the internal heat source is considered to be only due to polarisation heat (2) and the external source considered is the convection heat exchange with the ambient air (3)[46, 47]. Here, E and V_{ocv} represent respectively the operation voltage and the open circuit voltage. In this approach, any heat exchange due to radiation is ignored given the fact that, when located on the exterior, the BESS is protected from direct solar radiation and often includes heat management systems.

$$mC_p \frac{dT}{dt} = \frac{dQ_{int}}{dt} + \frac{dQ_{ext}}{dt} \quad (1)$$

$$\frac{dQ_{int}}{dt} = I \cdot (E - V_{ocv}) \quad (2)$$

$$\frac{dQ_{ext}}{dt} = \lambda \cdot A \cdot (T_{air} - T^B) \quad (3)$$

Using an equivalent circuit composed only of the internal resistance, the polarisation heat can be written as the ohmic loss in (4) where I is the DC

current in amperes. Incorporating this reformulation with the ambient heat transfer, we obtain a generalised thermal expression as shown in (5) that allows us to describe the intra-day behaviour of the battery by determining the internal resistance R_{int} and the ambient heat exchange coefficient λ . The heat capacity C_p could be obtained experimentally as it is not given by the manufacturer, but in reality this is not feasible as the conditions and tests would result in important unavailability periods for the BESS. Instead, this value is incorporated directly into the internal resistance and the heat exchange coefficients (R_{int}^* , λ^*) as seen in (5).

$$Q_{pol} = R_{int} \cdot I^2 \quad (4)$$

$$\frac{dT^B}{dt} = R_{int}^* I^2 + \lambda^* \left(T_{air}(t) - T^B(t) \right) \quad (5)$$

To estimate the values of the parameters R_{int}^* , λ^* , we can distinguish two scenarios: one with very low currents ($|I| \ll 1$) – and thus we can suppose a negligible internal heat generation in (6), and one with a high current ($|I| \gg 1$) in which the internal resistance loss dominates over the heat exchange with the environment (7).

$$\frac{dT^B}{dt} \approx \lambda^* \left(T_{air}(t) - T^B(t) \right) \quad \forall I \ll 1.0 \quad (6)$$

$$\frac{dT^B}{dt} \approx R_{int}^* I^2 \quad \forall I \gg 1.0 \quad (7)$$

$$R_{int}^* = \sum_m (b_+ \xi_{m,+} SoC^m + b_- \xi_{m,-} SoC^m) \quad (8)$$

As the parameter λ^* is solely dependent on the physical configuration and location of the BESS, this value can be obtained directly by interpolation from low current measurements.

For the internal resistance, given its dependency on the SoC and the charge/discharge regime, the parameter can be expressed as the polynomial $R_{int}^*(SoC, b_+, b_-)$ seen in (8) to better reflect the battery's behaviour. Here the variables b_+ , b_- represent binary values to indicate whether the power direction goes to (-, charge) or from (+, discharge) the batteries. The procedure shown in Algorithm 1 can be used to estimate the values of the parameters $\xi_{m,\{+,-\}}$ for R_{int}^* .

Algorithm 1 Find R_{int}^* polynomial

- 1: **procedure** $R_{int}(SoC, P_+^B, P_-^B)$
 - 2: Separate measurement datasets by regime: charge or discharge
 - 3: For each dataset:
 - 4: Separate continuous data by SoC range
 - 5: Select continuous measurements with low I
 - 6: Calculate average λ_{SoC}^*
 - 7: Select continuous datapoints with high I
 - 8: Calculate average $R_{int,SoC}^*$
 - 9: Do a polynomial fit on $R_{int,SoC}^*$
-

2.2.1. Maximum temperature prediction

As the risks of thermal runaway and degradation increase with extreme temperatures [14, 15, 48], it is important to predict the high or low temperatures that the battery cells can reach during operation. The focus in this work was on the maximal temperature that can be reached since the minimal temperature is practically limited by the ambient temperature.

The two approaches we propose for the prediction of the highest operating temperature were as follows: the maximal temperature is obtained using 1) an intra-day temperature estimation by eq. (5), and 2) a neural network that uses the average discharge power, discharge duration, and ambient temperature as input features (accessible independently from the BESS). Thanks to the regularity of the expected battery cycles in capacity firming frameworks, more sophisticated techniques such as recursive neural networks were not needed, although good results employing this method have been reported in the literature [49].

2.3. The SoC model

The model used to estimate the SoC is based on determining the charge/discharge efficiency η_I in the coulomb integrator shown in equation (9), but the AC power is used instead of the DC current as it is a value that is always available (observable) and independent from the BESS manufacturer. The initial battery capacity Ah_0 is then represented as the capacity E_0 in watt-hours. The impact of the internal temperature was taken into account and incorporated in the SoC estimator shown in (10) via the addition of parameter η_T . This supplementary term can be seen as a temperature-dependant self-discharge

rate which, in ECM terms, can be represented as a thermistor parallel to the voltage source [50].

$$\frac{dSoC}{dt} = \frac{\eta_I}{Ah_0} I \quad (9)$$

$$\frac{dSoC}{dt} = \frac{\eta_P P}{E_0} + \eta_T T^B \quad (10)$$

As reported in the literature, the performance depends on the power flow direction [51–53], and thus an approach similar to the one used for the internal resistance to estimate the battery’s operational temperature was used in equation (11) to distinguish between the charge and discharge performances ($\eta_{P,+}, \eta_{P,-}$).

$$\frac{dSoC}{dt} = \frac{\eta_{P,+} P_+ + \eta_{P,-} P_-}{E_0} + \eta_T T^B \quad (11)$$

The parametrisation can be done using standard operational data, requiring only the AC power and the SoC published by the battery’s BMS. If the internal temperature is available, then η_T can be also determined.

2.4. The SoH model

The ageing of battery cells can be separated into two different regimes: cyclic and calendar ageing, both of which are consequences of solid electrolyte interface (SEI) formation inside the cells [54]. Xu et al. in [55] expressed these behaviours using two SEI growth parameters α_{sei} , β_{sei} and a unit cycle deterioration function $f_{d,1}$ in eq. (12), with N being the number of full charge/discharge cycles the BESS has been subject to. This model is able to reproduce the fast initial degradation due to SEI formation thanks to the first term, and the continuous cycle-dependent degradation in the second. This approach is also not exigent in operational data, as only a health indicator and the AC power through the BESS is needed.

$$SoH = \alpha_{sei} e^{N\beta_{sei} f_{d,1}} + (1 - \alpha_{sei}) e^{-N f_{d,1}} \quad (12)$$

In this formulation, the individual calendar ageing is not expressed explicitly as it is included in the cycle degradation $f_{d,1}$ thanks to the regularity and homogeneity of the cycle duration in the dataset used in this work. For those cases where the case usage is not regular, it is possible to use expression f_d in eq. (13) to replace $N f_{d,1}$, where δ_i is the depth of discharge, σ_i is the

average SoC, and $T_{c,i}$ is the average temperature for the i th cycle. Traditional curve-fitting techniques can then be used to identify the parameters in equation (12) when cycle-induced degradation experiments are available.

$$f_d(t, \delta, \sigma, T_c) = f_t(t, \hat{\sigma}, \hat{T}_c) + \sum_i^N n_i f_c(\delta_i, \sigma_i, T_{c,i}) \quad (13)$$

A particular complication arises when working with operating hybrid sites as the cost in production loss from BESS unavailability is not negligible and degradation tests are rarely carried out. In addition, for large-scale systems, the BESS manufacturer provides a long-term maintenance service which includes regular repair and material replacement programs. Figure 1 shows the capacity retention (SoH) as reported by a BMS from the dataset during the first year of operation after commissioning, clearly displaying the off-line periods (SoH of zero), the malfunction of battery racks (decrease in SoH down to 70%) as well as the introduction of fresh cells (step increase in SoH seen for instance in cycles 45 and 60). The fitting procedure implicitly takes into account this human intervention, as only the absolute values and their sequential evolution are used.

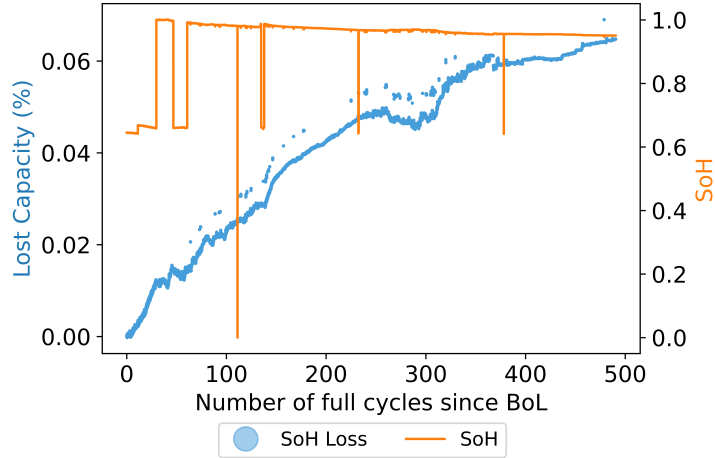


Figure 1: SoH and calculated loss in capacity as reported by the BMS used to parameterise the SoH model.

3. Optimisation of Hybrid PV Capacity Firming Sites

The PV capacity firming framework of interest in this study follows the constraints established by the French Energy Regulatory Commission for PV+Storage systems in insular French grids (AO CRE ZNI). The operation and power injection of such power plants are subject to the following constraints: day-ahead and intra-day power engagements with slope constraints, minimal and maximal power limits, and a remuneration scheme with penalties when power injection deviates from the published engagement. The evaluation time for these requirements is 1 minute, and the price per kWh is defined by the constructor when answering the call for tenders. A bonus of 200 €/MWh is applied to all the energy provided during a period of 2 hours, defined to be between 19:00 and 21h:00.

The possible power flow of such power plants can be visualised in figure 2. The injection into the grid P_i^G aims to respect a previously declared engagement E_i and is a direct response to the power injection from the solar resource P_i^S and storage P_i^S . Two different optimisations can be made as these power plants are subject to both day-ahead planning and real-time operation. The first is the optimal engagement (schedule) given a PV production forecast $P_{i,in}^S$, and the second is the optimal production given the real photovoltaic production and a previously defined schedule.

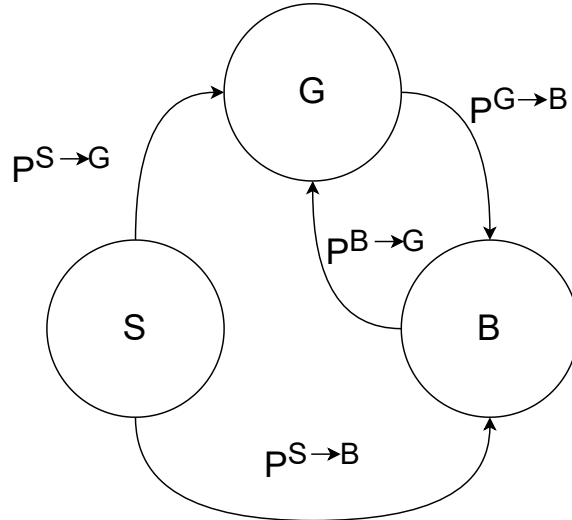


Figure 2: Power flow in the PV + Storage capacity firming power plants featured in this study.

The problem of optimal engagement in this PV capacity firming framework can be seen in equations (14). The constraints (14b-14c) establish the contractual limits and change rates $\Delta^{+,-}$ between consecutive engagement values. The objective function aims to maximise the revenue given the decision variable E_i and the penalty p dependent on the engagement and the grid injection.

Because the engagement is equivalent to the expected grid injection, the penalty p is expected to be zero as there is no deviation between the values. However this may not always be the case, as the engagement could be contractually obliged to produce a minimal value that is higher than what the storage can physically deliver.

$$\max \sum_n c_i^G * \left(E_i - p \left(E_i, P_i^G \right) \right) \quad (14a)$$

s.t.

$$E_{i,min} \leq E_i \leq E_{i,max} \quad \forall i \quad (14b)$$

$$\Delta^- \leq E_{i+1} - E_i \leq \Delta^+ \quad \forall i \quad (14c)$$

$$E_i = P_i^{S,in} + P_i^B \quad \forall i \quad (14d)$$

$$P_i^G = E_i \quad \forall i \quad (14e)$$

$$P_{i,min}^B \leq P_i^B \leq P_{i,max}^B \quad \forall i \quad (14f)$$

$$P_{i,min}^G \leq P_i^G \leq P_{i,max}^G \quad \forall i \quad (14g)$$

$$SoC_{i+1} = f(SoC_i, P_i^B) \quad \forall i \quad (14h)$$

$$0 \leq SoC_i \leq 1 \quad \forall i \quad (14i)$$

In the case of optimal grid injection with a predefined engagement, the driving decision variables are the solar and storage output power P_i^S, P_i^B . In this case $P_{i,in}^S$ does not represent the expected solar production but rather the real solar production that might need to be curtailed. This optimisation problem, which also aims to maximise the revenue, can be seen in (15).

$$\max \sum_n c_i^G * \left(E_i - p \left(E_i, P_i^G \right) \right) \quad (15a)$$

s.t.

$$P_i^G = P_i^S + P_i^B \quad \forall i \quad (15b)$$

$$0.0 \leq P^S \leq P_{i,in}^S \quad \forall i \quad (15c)$$

$$P_{i,min}^B \leq P_i^B \leq P_{i,max}^B \quad \forall i \quad (15d)$$

$$P_{i,min}^G \leq P_i^G \leq P_{i,max}^G \quad \forall i \quad (15e)$$

$$SoC_{i+1} = f(SoC_i, P_i^B) \quad \forall i \quad (15f)$$

$$0 \leq SoC_i \leq 1 \quad \forall i \quad (15g)$$

In both scenarios presented, the BESS SoC model plays a crucial role as it determines the total output of energy and power available. By including the thermal behaviour in (15f), the optimal engagement reduces the thermal stress to maximise the total energy engagement. For the optimal operation, thermal consideration would arbitrate between the penalty and the loss in performance of the BESS.

4. Optimisation of an Ensemble of Grid-connected BESSs

To showcase the applicability of the BESS models developed under the discussed PV capacity firming scenario, a different use case was also studied. The optimisation paradigm here aims to solve the problem of managing multiple BESS connected to a low voltage (LV) network. The types of algorithm that allow this operation have been referred to in the past as Network Battery Aggregators (NBA) [56], and this name will be adopted in this work.

The scenario showcased in this NBA algorithm is one where, given a load L at an instant i , we try to minimise the cost of energy by using the storage systems and a vRES present in the network. In this case, the energy is considered to come from a photovoltaic power plant $P_i^{S,in}$, and it is expected to be manageable to allow production curtailment if needed P_i^{S*} . Figure 3 summarises the possible power flows in the system.

The scenario here presented can recognise an arbitrary number j of batteries, each with a unique thermal and SoC behaviour described by the functions $g^j(T_i^j, SoC^j, P^j)$, $f^j(T^j, SoC^j, P^j)$ for which the parameters can be found

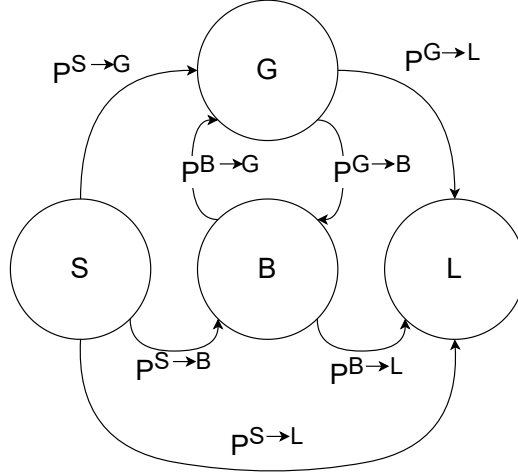


Figure 3: Power flow represented in the optimisation problem. The power superscripts (source, destination) represent the direction of the power P , assumed to be always positive or greater than zero.

as described in section 2. Furthermore, by repeating the optimisation with an additional grid power requirement, the framework allows us to quantify the cost of the local flexibility provided by the BESS. This is explained in detail in section 3.1 below.

The inclusion of an estimation of the intra-day temperature in this framework then results in the non-linear problem (NLP) seen in (16), which modern solvers are able to solve. In this representation, PV curtailment is allowed thanks to the constraint (16f), and BESS power is maintained between limits by the constraint (16h). The temperature and SoC functions are defined by their discrete versions, which can be seen in equation (5) for the former and equation (11) for the latter.

$$\min \sum_{i=1}^n \left(c_i^G P_i^G + c_i^S P_i^S + c_i^{S*} P_i^{S*} + c^B P_i^B \right) \quad (16a)$$

$$\text{s.t.} \quad P_i^G = L_i - P_i^S - P_i^B, \quad \forall i, \quad (16b)$$

$$P_i^S = P_i^{S \to G} + P_i^{S \to L} \quad \forall i, \quad (16c)$$

$$P_i^B = \sum_j P_i^{j \to L} \quad \forall i, \forall j, \quad (16d)$$

$$P_i^{S \rightarrow B} = \sum_j P_i^{S \rightarrow j} \quad \forall i, \forall j, \quad (16e)$$

$$P_i^{S*} = P_{i,in}^S - \left(P_i^{S \rightarrow G} + P_i^{S \rightarrow B} + P_i^{S \rightarrow L} \right) \quad \forall i, \forall j, \quad (16f)$$

$$P_i^j = P_i^{S \rightarrow j} - P_i^{j \rightarrow L} \quad \forall i, \forall j, \quad (16g)$$

$$P_{min}^j \leq P_i^j \leq P_{max}^j \quad \forall i, \forall j, \quad (16h)$$

$$SoC_{i+1}^j = f(T_i^j, SoC_i^j) \quad \forall i, \forall j, \quad (16i)$$

$$T_{i+1}^j = g(T_i^j, SoC_i^j) \quad \forall i, \forall j \quad (16j)$$

However, when using the originally proposed SoC and temperature equations the non-linearity of the problem was too extreme and convergence was found to be irregular and unreliable. A simplification of functions (16i), (16j) was done to reduce non-linearity as follows: in the SoC equation the different charge/discharge parameters were merged into a single round-trip efficiency parameter in eq. (17), and for the thermal equation the internal resistance was averaged over the SoC range of operation as in (18).

$$SoC_{i+1}^j = SoC_i^j + \eta_T T_i^j + \eta_P P_i^j \quad (17)$$

$$T_{i+1}^j = T_i^j + \bar{R}_{int}^{*,j} I_i^{j2} + \bar{\lambda}^{*,j} (T_{ext,i} - T_i^j) \quad (18)$$

4.1. Flexibility evaluation in the optimisation framework

As mentioned above, an effort is made to incorporate into the optimisation problem and then evaluate the cost of flexibility offered by the storage, and to measure the impact the thermal model would have on this scenario. To accomplish this, the same structure as discussed in (16) was used, with the addition of the constraint below:

$$P_i^G = K \quad \forall i \in t_e \quad (19)$$

$$K = 0 \quad \forall i \notin t_e \quad (20)$$

This last addition imposes the power injected into the grid at a value K for each instant in the period of time t_e , which is equivalent to a request for power injection or withdrawal from the grid. Respect of this constraint was evaluated with the new objective function in (21) as the difference between this value and the power flow from the grid, and thus in this period t_e the

Table 1: Data availability for each of the BESS in the collection setups. Y indicates available and N not available.

BESS	Wh/Wc Ratio	Thermal Model	SoC Model	SoH Data
#1	1.35	N	Y	Y
#2	1.43	N	Y	Y
#3	1.39	N	Y	Y
#4	1.36	N	Y	Y
#5	0.87	Y	Y	N
#6	0.87	Y	Y	N
#7	0.87	Y	Y	N

cost is associated with this unmet grid power request and the LCOE from the resources engaged.

$$\sum_{i=1}^n \left(c_i^G |P_i^G - K| + c_i^S P_i^S + c_i^{S*} P_i^{S*} + c^B P_i^B \right) \quad (21)$$

5. Results

5.1. Experimental data collection setup

The BESS measurements were collected for the period between 2020 and mid-2021 from 5 different hybrid photovoltaic power plants with different ratios of installed capacity per installed PV power (Wh/Wc). These plants are located on the island of Corsica and in continental France, and each one follows the PV capacity framework previously discussed in section 3. The data are saved with a periodicity of one second by the local SCADA of each hybrid plant developed on the platform *Ignition*, which itself recovers the information through the protocol Modbus TCP/IP. All power-related measurements were obtained directly from each production system’s communication interface (BESS or PV plant), which results in datasets with different reliability and refresh rates depending on the manufacturer. Table 1 summarises the possible models and usages available per BESS.

The collected data were used both for model training/parameterisation and validation, using a ratio of 2:1. For all the models, the data per second were averaged to a timestep of 1 minute.

A detailed view of the information in such datasets can be seen in Appendix A; they were subject to filters to avoid aberrant days when the grid’s point of common coupling (PCC) was unavailable.

Table 2: Convection heat exchange coefficients

BESS	#5	#6	#7
R_{int}^*	5.928×10^{-7}	4.03×10^{-7}	4.808×10^{-7}
λ^*	1.12×10^{-4}	6.76×10^{-4}	9.84×10^{-4}

5.2. Thermal model error

The thermal parameters $\xi_{m,+}$, $\xi_{m,-}$, λ^* were calculated for those BESS that provide internal temperature measurements by using the reported current in DC. The convection heat exchange coefficient and average internal resistance found for the batteries can be seen in Table 2.

The error resulting from using the parameters in the temperature model was found to be less than 1 °C on average for a 1-day horizon. When using the model to estimate 7 continuous days, the average error increased to ≈ 2 °C. Figure 4 shows the estimated and measured temperatures for one of the BESS. The general behaviour of the estimation follows the real measured values, although the model is unable to reproduce more subtle changes as the midday temperature increases.

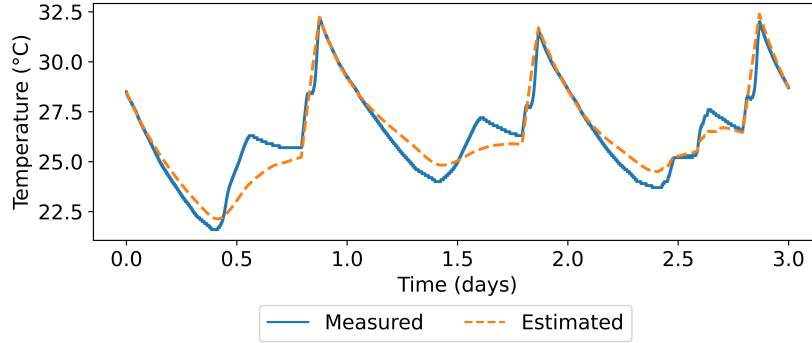


Figure 4: Internal temperature prediction for one of the BESS.

5.2.1. Maximal Temperature Predictor

The intra-day temperature model in eq. 5 showed an average error of 2.31 °C for the maximal daily temperature. When using the trained neural network maximal temperature predictor, these errors were reduced to an

average of 0.9 °C. Figure 5 illustrates the results for both approaches and displays the higher error of the intra-day temperature model.

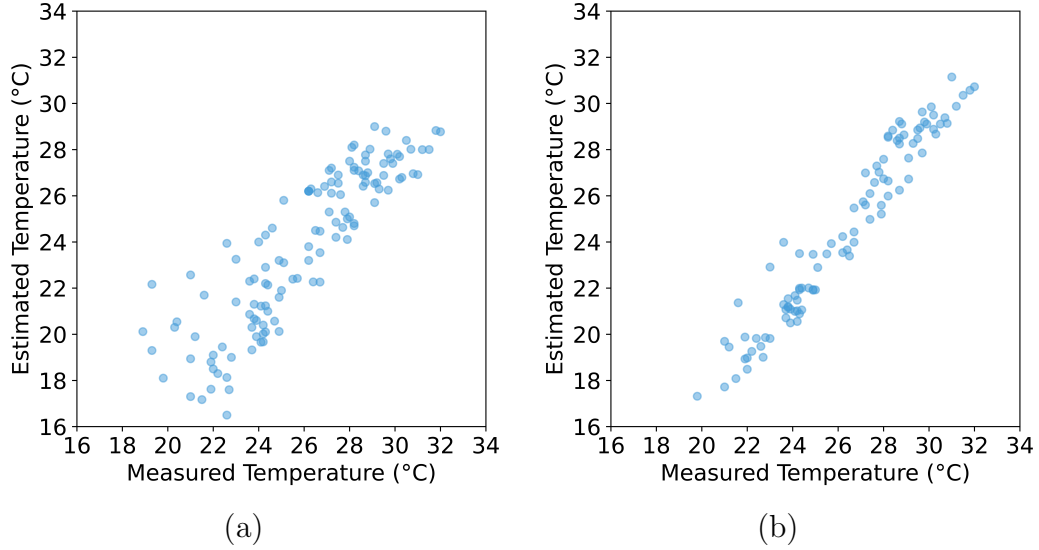


Figure 5: Maximal temperature prediction using intra-day estimation (a) and a neural network technique (b).

5.3. SoC model

The improved SoC models showed a consistent upgrade in error reduction when compared to a base model that uses the manufacturer base performance value. The manufacturer’s reported round-trip efficiency fails to accurately reflect the loss in performance in a charge regime, and thus generates a cumulative error that tends to under-estimate the remaining capacity available in the BESS. Table 3 shows the round-trip parameters found for the studied BESS based on the procedure previously explained. In all scenarios, the real round-trip efficiency was systematically lower than the manufacturer value.

Table 3: Round-trip efficiency found for each SoC trained model.

BESS	#1	#2	#3	#4	#5	#6	#7
η_P	90.12%	88.52%	88.55%	87.85%	83.96%	80.95%	82.57%
Factory η_P	92.00%	92.00%	92.00%	92.00%	95.00%	95.00%	95.00%

When considering a horizon of 7 continuous days, the error in SoC estimation when using the factory-issued η_P can reach up to 30%. If the horizon is constrained to a single day, this error is onaverage 12%. In both scenarios, using the improved parameterised SoC model with no thermal dependence reduced the average error by more than 60%, reducing the average daily mean absolute error (MAE) to $\approx 3\%$ for the 7-day period and $\approx 1\%$ for a single day. The error distributions for the 7-day periods can be seen in Figure 6.

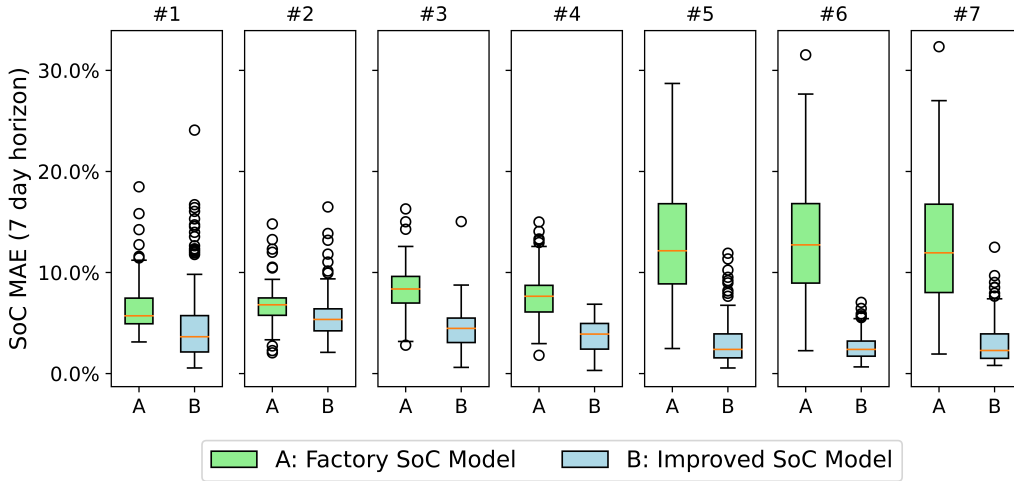


Figure 6: RMSE distribution for 7-day continuous SoC estimation without thermal consideration for each BESS.

5.3.1. SoC and thermal model coupling

As the SoC model in equation (10) uses the BESS temperature to determine a self-discharge component, any implementation in scheduling or control processes would need to estimate the temperature component as well. This was done using the model and parameters discussed in section 5.2 for the relevant BESS. Nevertheless, the relationship between temperature and SoC is not symmetrical: the temperature estimation was unaffected by the error introduced by the SoC model, but the SoC did show an increase in accuracy when using an estimated internal battery temperature. This change however was very small ($<1\%$ in SoC error reduction), and opens the possibility of explicitly ignoring the parameter if there is no need for a higher degree of precision.

5.4. SoH model

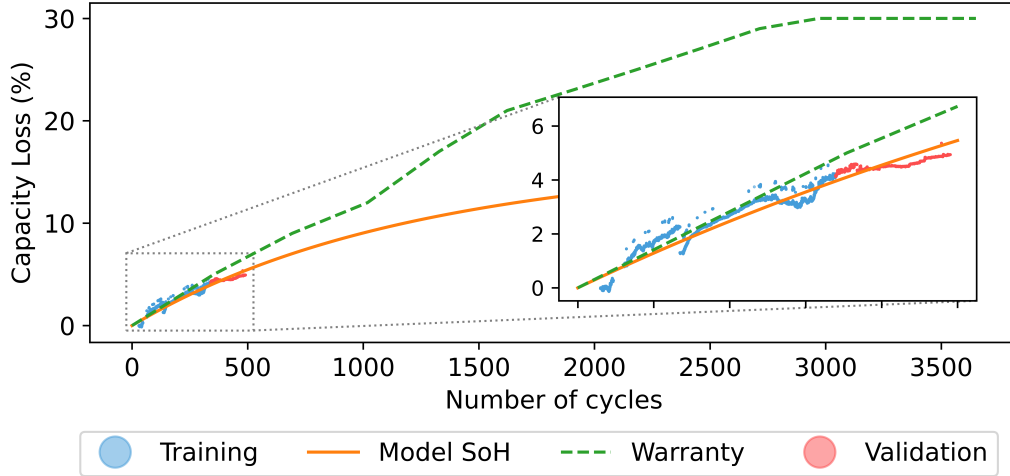


Figure 7: Predicted SoH for one BESS in a 2-year horizon. The blue dots represent the training set, and the red dots the validation set.

Equation (12) was parameterised for BESS 1-4 since these systems provide the data needed for the model. The results can be seen in Table 4, and they describe the expected SoH evolution given the constant cycling behaviour associated with the PV capacity firming framework that the sites follow. In half of the cases, these values showed the strong expected initial degradation linked to SEI formation, going up to 5% energy capacity loss in the first year when considering an average of 1 cycle per day, as well as the subsequent softer degradation.

The expected degradation over 10 years of cycles for one of the BESS can be seen in Figure 7, where the broken green line indicates the maximal capacity loss accepted by the manufacturer’s warranty. As previously mentioned in section 5.1, the training data to determine the parameters presented here came from the first year of operation. When reducing the amount of training data to less than a year, the SoH model predicted behaviour similar to the warranty loss because the SEI formation phase was still predominant.

5.5. Optimisation framework results

The development and programming of the different NLP problems presented above was done using Python’s Pyomo interface [57, 58], and the

Table 4: Degradation parameters

BESS	α_{sei}	β_{sei}	$f_{d,1}$
#1	0.1440	148.85	6.02e-06
#2	0.002	0.961	1.2e-04
#3	0.4907	129.95	3.19e-06
#4	0.0490	149.99	1.93e-06

solver IPOPT was used to find the optimal solution [59]. The BESS models implemented were a simple perfect charge/discharge process ($\eta_P = 1$), a factory SoC model ($\eta_P = \text{Factory-issued value}$), and an improved SoC model (parameterised η_P). This latter could be employed with or without explicit thermal dependence by establishing the value of η_T .

The results from each framework and the specific constants taken into account are shown below.

5.5.1. PV capacity firming with advanced BESS modelling

The BESS models studied in this scenario correspond to the improved SoC model without thermal dependence. These values were compared to the optimisation framework results when the factory SoC model is used. The BESS used in this framework were systems #1-#4, as they offer both SoC and SoH data to parameterise the models. For all sites, the initial SoH was considered to be at 1 year of full cycles as estimated by its own SoH model.

The energy price c^G was set to 100€/MWh, which is 50% of the bonus of 200€/MWh used in the AO CRE ZNI framework for any injection between 19:00 and 21:00. The timestep studied was set to one minute with a one-day horizon as required by the framework. The PV production scenarios, as well as a standard PV production forecast for the optimal engagement, can be seen in Appendix B.

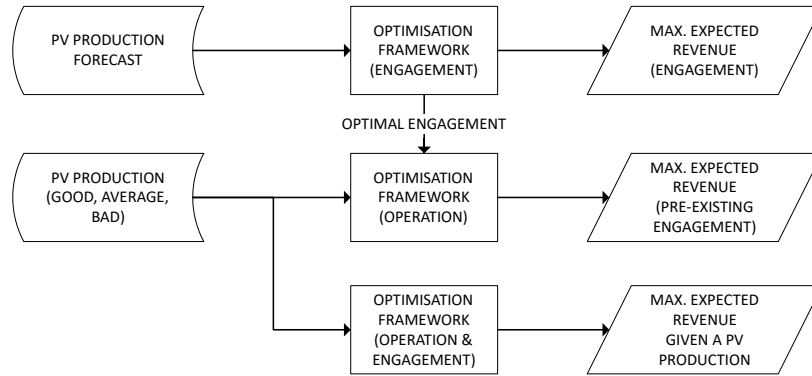


Figure 8: Workflow used for the different optimisation scenarios.

The estimated remunerations were evaluated for the following scenarios:

1. The optimal engagement strategy given a PV production forecast.
2. The optimal operation given the previously determined engagement and real PV production.
3. The optimal engagement and operation given the PV production.

The procedure can be seen in Figure 8. For all scenarios, the SoH loss evolution between BESS models was evaluated.

5.5.2. Optimal engagement

The different expected revenues followed the charge/discharge performance found in the improved SoC model. The change in expected revenue, seen in Table 5, increased for the BESS, for which the discharge process is more efficient than the value published by the manufacturer. Inversely, the expected revenue decreased for those that exhibited a weaker performance in the improved SoC.

Table 5: Revenue improvement by using the improved SoC model with an optimal engagement given a PV production forecast.

	BESS						
	#1	#2	#3	#4	#5	#6	#7
Δ Revenue	0.3%	-0.7%	-1.9%	-1.9%	-1.09%	-1.47%	-1.29%

5.5.3. Optimal operation

Once an optimal engagement and revenue had been generated using the PV production forecast, the expected maximal revenue based on this engagement and an observed solar production was calculated. Figure 9 shows the change in revenue observed per type of solar behaviour.

In all scenarios except for one BESS, the revenue decreased systematically when using the improved SoC model. This decrease in revenue due to the BESS model was similar for both the cases of good and average solar production, and the financial impact only surpassed 10% in the case in which the solar variation was very high (bad case).

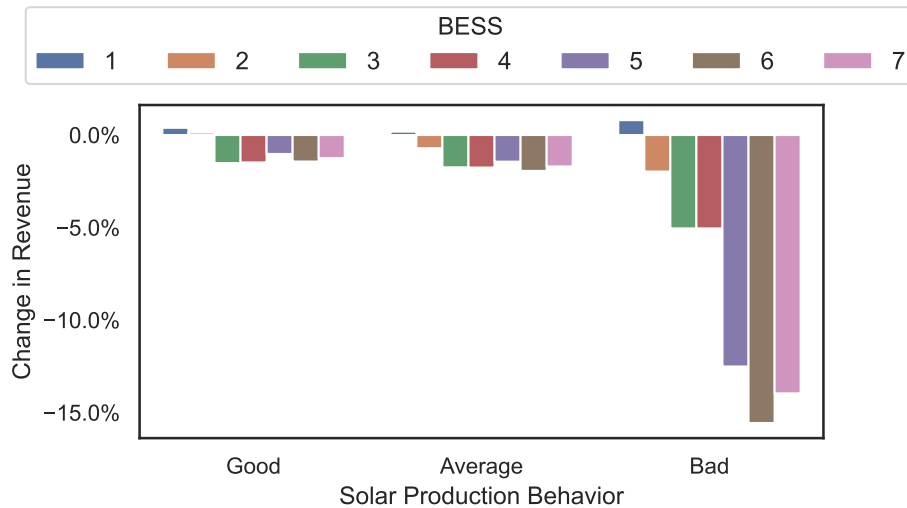


Figure 9: Expected change in optimal revenue given the improved SoC model under different solar scenarios. The engagement was defined beforehand.

5.5.4. Optimal engagement and operation (known PV production)

In the case where the optimisation framework attempts to maximise the revenue given a specific solar production, i.e. the maximal possible revenue that a system could attain if given a perfect PV production forecast, the improved SoC model decreased the revenue as in the previous cases (see Figure 10). The average decrease in revenue for all sites and all weathers employing the BESS model was 1.602%, which is 50% less impact than the case in the precedent section 5.5.3.

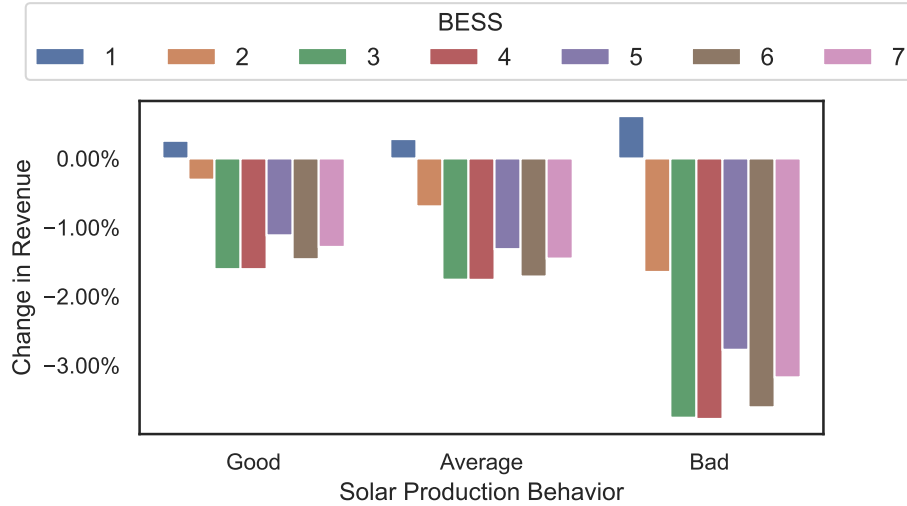


Figure 10: Expected change in optimal revenue employing the improved SoC model under different solar scenarios. The engagement was defined given the solar scenario.

5.5.5. State of Health loss

In this optimisation framework, the loss of SoH was calculated for the four BESS systems for which the SoH model in section 5.4 was parameterised. The use of the improved SoC model instead of the factory-issued model increased the expected capacity loss by $>2.5\%$, and the increase per scenario and BESS can be seen in Figure 11.

On a daily basis, the cost due to the SoH loss represented on average 0.0078% of the initial cost of the system. Using the improved SoC model increased the cost to 0.0081%. For similar cycles during a 10-year period, according to the behaviour expected from the AO CRE ZNI PV capacity framework sites, the cumulative capacity loss would increase from 28.5% to 29.6%.

5.6. Battery aggregation optimisation

The developed BESS models shown in this work, although trained using data from experimental sites that follow a very specific PV capacity firming behaviour, were subjected to the battery aggregation scenario previously discussed in order to test applicability in other use-cases. For this scenario, three distinct BESS models were tested when the coupled renewable energy source, a PV power plant, has the different solar productions shown in Appendix B.

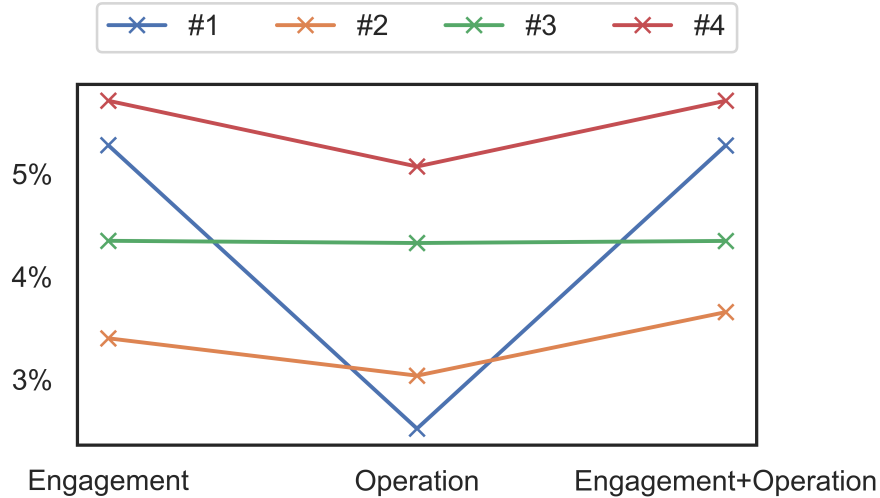


Figure 11: Increased loss of SoH per BESS under the three different optimisation objectives and with the improved SoC model. The base value is the SoH loss when using the factory SoC model.

The evaluation timeframe was restricted to a 1-day horizon with a 10-minute timestep, and the cost associated with each MWh per energy source was set as follows: 400€ for the grid, 70€ for the photovoltaic plant, 140€ for unexploited photovoltaic energy, and 120€ for the storage. The temporal resolution was set to reflect the variable behaviour of the solar resource, phenomena that are often softened when using longer timesteps. This is important given that short-term power requirements from the BESS can be masked in such timeframes and by consequence hide the thermal stress.

The BESS models used were the factory-issued SoC model (as a reference) and the improved SoC model with and without temperature dependence. They were implemented in the optimisation framework described in section 4 and results were analysed through the cost of energy to satisfy the local load and the cumulative expected capacity loss from the BESS. Table 6 summarises the cumulative capacity loss for all attached BESS in the three weather scenarios, and Figure 12 shows the specific SoH loss per BESS. The initial temperature of such systems was similar (15.9, 17.1, 16.5 °C) and the initial degradation state was considered to amount to 2 years of cycles ($N = 720$, an average of 1 cycle per day). The equation (22) was used to obtain

Table 6: Cumulated SoH Loss change by weather model. Less is better.

Day	Factory SoC (Reference Value)	Improved SoC (change %)	Improved SoC + T (change %)
Good	0.0223%	5.01%	4.68%
Average	0.0217%	5.12%	4.75%
Bad	0.0221%	1.80%	1.79%

the results, with N_i being the cycles featured in BESS i in the resulting optimisation.

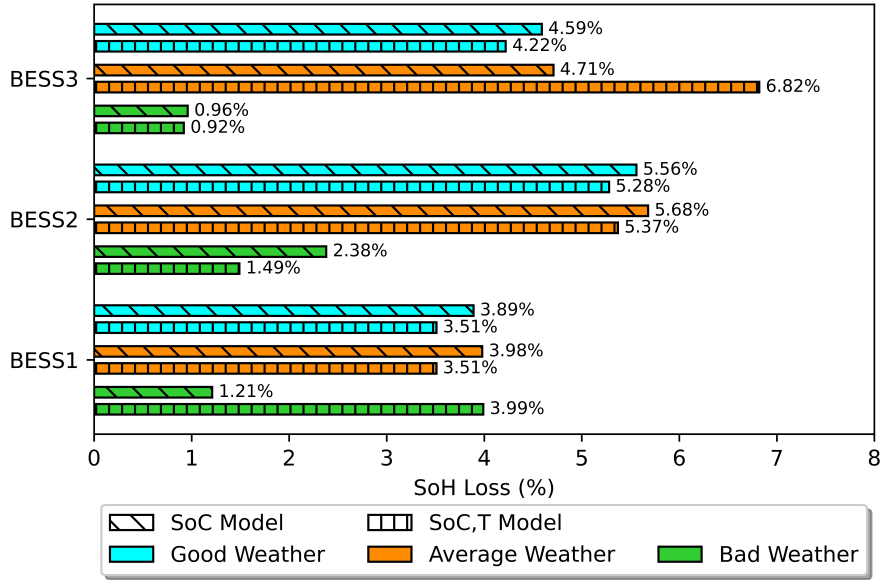


Figure 12: SoH loss per BESS in the optimisation problem when using different SoC models and in different weather.

In the three scenarios, the improved SoC model increased the estimated degradation in the different BESS due to the higher energy throughput needed to fully charge the batteries. As the efficiency is below the factory-issued performance, this value was naturally higher than in the reference SoC model. When integrating the temperature component in the SoC, the

expected loss was lower than in the case were it is not included.

$$SoH_{Loss} = \sum_{i=1}^3 SoH(N) - SoH(N + N_i) \quad (22)$$

5.6.1. Flexibility cost

The flexibility framework described in section 4.1 was only studied under the good PV production scenario. The added flexibility requirement was found to increase the energy price by up to 10% when the energy demand constituted 40% of the installed PV capacity. Figure 13 shows the increase in price when using the improved SoC model with intra-day temperature prediction instead of the standard factory-issued SoC model. Both grid power withdrawal and injection requirement have a similar impact on absolute cost, the former being only slightly higher. As a result of requesting energy absorption capability, solar resources are necessarily wasted and the number of cycles in the BESS increases.

The specific impact of the intra-day temperature on the optimisation framework was however not significant enough. The energy cost difference between the scenarios with and without temperature was small ($< +0.1\%$), and including the cost due to BESS degradation did not change this gap. As the thermal degradation is not included in the objective function, the SoH loss is not optimised and only the energy throughput is taken into account.

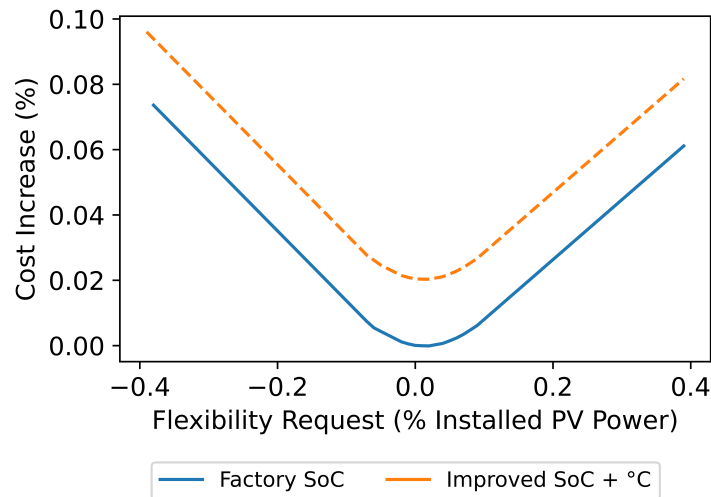


Figure 13: Increase (in %) of energy cost when imposing a flexibility constraint with different storage models.

6. Conclusion and Discussion

In this work, we dealt with the subject of battery modelling and parameterisation to determine the operational SoC, SoH and temperature of BESS using only common, industrially available measurements. The models were validated with in-situ data extracted from 5 different hybrid PV power plants (7 BESS in total), and revealed a general improvement in SoC and SoH estimation. Given that BESS manufacturers do not provide thermal predictor models, the temperature was compared to measured values only. This thermal difference was found to be less than 2 °C, a difference small enough to ensure that thermal management can avoid any overheating of the system by integrating the developed model. The general simplicity of the models makes them easy to integrate into more advanced applications, and then measure the impact of temperature on battery degradation and management.

The state-of-charge model was trained using the available power and the SoC values reported by the factory BMS. When temperature measurements were available, the thermal impact was expressed as a temperature-dependent self-discharge parameter. The inclusion of this parameter in SoC estimation reduced the average error of the model by 2%.

Lastly, the state-of-health model was also parameterised with the available data and showed a degradation trend below the warranty provided by the different BESS. When using a smaller set of data, as would be the case for the early years of hybrid projects, the trend followed a similar pattern to the constructor's expected capacity. If data beyond the first year are included, then the model better reflects the real behaviour.

By using both the warranty for capacity retention and the predicted SoH loss from the model, hybrid power plant investors have a set of scenarios to adhere to and perform further analysis. A pessimistic approach could use the warranty values published by the BESS manufacturer, while an optimistic one would follow the newly parameterised curve. A finer risk management strategy can then be introduced by selecting a curve that falls between the two.

An additional convenience of the models is also the low computational load they require, taking between 5-10 seconds on an intel i7-7700HQ to parameterise. Coulomb counting, OCV approaches, and ECM require the least amount of measurements and the lowest computational effort compared to observers and KF [60]. This allows them to run on light industrial computers on remote sites. Moreover, the results obtained by the models were coherent

with the reported errors in the literature for similar estimation techniques. For SoC, the average errors found throughout the literature range between 1% and 6% [61, 62] depending on the cell chemistry, while for SoH, the MAEs found were less than 6% [60, 63]. It is important however to use data from the BESS of interest. The SoH model in [64] applied to the batteries in this work showed a MAE between 1-2%, contrasting with the less than 1% from the model here presented. This similarity in results provides further reasons to take similar modelling approaches in the considered industrial use-case regardless of the cell thanks to the parameters which are estimated from measurements. For this reason, the modelling is agnostic to the battery chemistry.

After validation of the different models, two different optimisation frameworks were built to analyse the impact the improved BESS modelling has on financial results and on the life expectancy of batteries. These focused on the problem of scheduling and optimal operation in hybrid PV capacity firming plants and in a micro-grid scenario with multiple BESS and a vRES.

In the first framework, which follows the AO CRE ZNI PV capacity firming constraints, the inclusion of the improved BESS model reduced the daily maximal expected revenue by at least 2%. This financial impact grew as the vRES behaviour became more erratic, reaching up to 15% for some of the BESS studied. In all cases, the revenue change was proportional to the BESS charge/discharge performance and, even when the operation was optimal, the change in revenue was unavoidable. Investors and hybrid PV power plant constructors could demand time-dependent charge and discharge performance warranties from BESS manufacturers to constrain this risk of revenue loss.

In the case of the micro-grid with battery aggregation, the SoC and the thermal model were included to propose optimal BESS usage, and the cost per energy source was chosen to promote the use of local resources. The total cost to satisfy the local load increased when considering the improved SoC alone, and increased again after explicitly adding the thermal behaviour to the BESS models. When analysing the capacity loss, the degradation was slightly less than when the improved SoC incorporated the temperature dependence. These results suggest that not incorporating the thermal component in scheduling optimisations can penalise life-time financial projections by overly estimating the storage degradation. Nevertheless, this deviation is estimated to be up to 0.5% of the capacity at the end of a 10-year cycle, which has a relatively low financial impact for BESS of less than 1MWh.

Using an SoH model such as the one developed in this work would be enough to reduce degradation over-estimations.

The optimisation framework was also used to evaluate the cost of flexibility and the impact that thermal consideration has on it. The results showed a higher cost when energy withdrawal is requested by the grid instead of injection, as well as a low-changing zone that corresponds to energy that can be given by the vRES or consumed by the local load. It did not however show a strong response to the thermal component, and when thermal optimisation was not taken into account the results were fairly similar.

Given the results obtained, explicit inclusion and calculation of intra-day temperatures in scheduling does not seem necessary, as the error the model introduces falls largely within the standard range of day-ahead forecast errors. It could be of interest to explore loads in which an explicit thermal component starts to have a stronger impact on energetic and financial performance. This effect was not strongly observed in this work, probably due to the relatively low power requirements of the load. More extreme scenarios featuring the need for much higher instantaneous BESS power could benefit from temperature optimisation.

Further studies will consider sizing BESS for mini-grid structures while taking into account intra-day temperature behaviour. In addition, different usage scenarios will be applied to determine the limits at which the intra-day temperature starts to become crucial in scheduling frameworks.

Appendix A. Collected Dataset

The structure of the daily datasets can be seen below:

1. s : second in the day (1 - 86,400).
2. t_{BoL} : time in years since BOL
3. SoC : inst. SoC
4. SoC^{kWh} : inst. SoC relative to nameplate capacity
5. P_B : inst. AC power reported by BMS in kW
6. P_{CM} : inst. AC power measured by power monitor
7. E_{kWh} : inst. energy stored reported by BMS in kWh
8. E_{max} : inst. maximal capacity reported by BMS in kWh
9. E_{out} : accumulated output energy in kWh
10. V_{DC} : inst. DC voltage reported by the BMS in V
11. I_{DC} : inst. DC current reported by the BMS in A
12. I_{DC}^2 : inst. squared DC current
13. $T_{ext,1}$: ambient temperature reported by sensor in °C
14. $T_{ext,2}$: ambient temperature reported by sensor in °C
15. T_{BESS} : BESS temperature reported by BMS in °C
16. P_B^+ : inst. positive AC power reported by BMS in kW
17. P_B^- : inst. negative AC power reported by BMS in kW

Of the seven different BESS, four BMS do not provide any low-level information (DC voltage, DC current, internal temperature) and instead publish values estimated from their own internal battery models.

Missing or unavailable values are marked as NaN and are the first criterion to reject a day's data from the model construction.

Appendix B. Weather Models

The different PV production profiles used in the optimisation framework can be seen in figure B.14. They represent the main three kinds of irradiation a photovoltaic central experiences: A clear-sky day, a moderate cloudy day, and an extremely cloudy day.

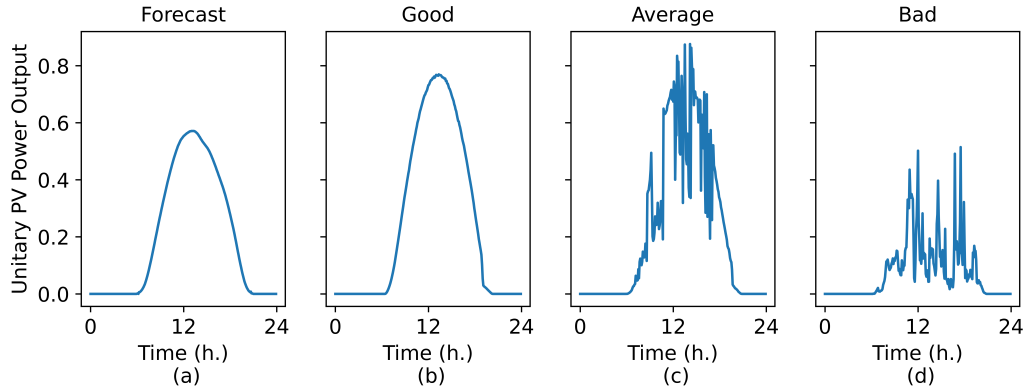


Figure B.14: PV production forecast (a) and three different behaviours of PV production for good (b), average (c) and bad (d) weather.

Acknowledgment

The authors would like to thank SPIE Industrie and the French government program CIFRE for financing the PhD research on this subject. They would also like to thank GDS Generale du Solaire for their measurements collected on selected hybrid sites.

References

- [1] Robert Gross, Tim Green, Matthew Leach, Jim Skea, Philip Heptonstall, and Dennis Anderson. The Costs and Impacts of Intermittency: An assessment of the evidence on the costs and impacts of intermittent generation on the British electricity network. Technical report, UKERC, 2006.
- [2] Philip Heptonstall, Robert Gross, and Florian Steiner. The costs and impacts of intermittency – 2016 update: A systematic review of the evidence on the costs and impacts of intermittent electricity generation technologies. Technical Report February, UK Energy Research Centre, 2017.

-
- [3] J. Skea, D. Anderson, T. Green, R. Gross, P. Heptonstall, and M. Leach. Intermittent renewable generation and the cost of maintaining power system reliability. *IET Generation, Transmission and Distribution*, 2(1):82–89, 2008. doi: 10.1049/iet-gtd:20070023.
- [4] Richard Green and Nicholas Vasilakos. Market behaviour with large amounts of intermittent generation. *Energy Policy*, 38(7):3211–3220, jul 2010. doi: 10.1016/j.enpol.2009.07.038.
- [5] Lynn Trahey, Fikile R. Brushett, Nitash P. Balsara, Gerbrand Ceder, Lei Cheng, Yet-Ming Chiang, Nathan T. Hahn, Brian J. Ingram, Shelley D. Minter, Jeffrey S. Moore, Karl T. Mueller, Linda F. Nazar, Kristin A. Persson, Donald J. Siegel, Kang Xu, Kevin R. Zavadil, Venkat Srinivasan, and George W. Crabtree. Energy storage emerging: A perspective from the Joint Center for Energy Storage Research. *Proceedings of the National Academy of Sciences*, 117(23):12550–12557, jun 2020. doi: 10.1073/pnas.1821672117.
- [6] Wesley J. Cole, Cara Marcy, Venkat K. Krishnan, and Robert Margolis. Utility-scale lithium-ion storage cost projections for use in capacity expansion models. In *2016 North American Power Symposium (NAPS)*, pages 1–6. IEEE, sep 2016. doi: 10.1109/NAPS.2016.7747866.
- [7] Wesley Cole, A Will Frazier, and Chad Augustine. Cost Projections for Utility-Scale Battery Storage: 2021 Update. Technical Report June, NREL, 2021.
- [8] Geoffrey J. May, Alistair Davidson, and Boris Monahov. Lead batteries for utility energy storage: A review. *Journal of Energy Storage*, 15:145–157, 2018. doi: 10.1016/j.est.2017.11.008.
- [9] Kudakwashe Chayambuka, Grietus Mulder, Dmitri L. Danilov, and Peter H. L. Notten. From Li-Ion Batteries toward Na-Ion Chemistries: Challenges and Opportunities. *Advanced Energy Materials*, 10(38):2001310, oct 2020. doi: 10.1002/aenm.202001310.
- [10] IRENA. Electricity storage and renewables: Costs and markets to 2030. Technical Report October, International Renewables Energy Agency, 2017.
- [11] G. Delille, B. François, and G. Malarange. Dynamic frequency control support by energy storage to reduce the impact of wind and solar generation on isolated power system’s inertia. *IEEE Transactions on Sustainable Energy*, 3(4):931–939, 2012. doi: 10.1109/TSTE.2012.2205025.

-
- [12] Oliver Schmidt, Sylvain Melchior, Adam Hawkes, and Iain Staffell. Projecting the Future Levelized Cost of Electricity Storage Technologies. *Joule*, 3(1):81–100, jan 2019. doi: 10.1016/j.joule.2018.12.008.
- [13] Ashreeta Prasanna, Kevin Mccabe, Ben Sigrin, and Nate Blair. Storage Futures Study - Distributed Solar and Storage Outlook: Methodology and Scenarios. *National Renewable Energy Laboratory (NREL)*, (July), 2021.
- [14] Todd M Bandhauer, Srinivas Garimella, and Thomas F Fuller. A Critical Review of Thermal Issues in Lithium-Ion Batteries. *Journal of The Electrochemical Society*, 158(3):R1, 2011. doi: 10.1149/1.3515880.
- [15] Languang Lu, Xuebing Han, Jianqiu Li, Jianfeng Hua, and Minggao Ouyang. A review on the key issues for lithium-ion battery management in electric vehicles. *Journal of Power Sources*, 226:272–288, mar 2013. doi: 10.1016/j.jpowsour.2012.10.060.
- [16] Matthew T. Lawder, Bharatkumar Suthar, Paul W C Northrop, Sumitava De, C Michael Hoff, Olivia Leitermann, Mariesa L Crow, Shriram Santhanagopalan, and Venkat R Subramanian. Battery Energy Storage System (BESS) and Battery Management System (BMS) for Grid-Scale Applications. *Proceedings of the IEEE*, 102(6):1014–1030, jun 2014. doi: 10.1109/JPROC.2014.2317451.
- [17] Max Jung and Simon Schwunk. High End Battery Management Systems for Renewable Energy and EV Applications. *Green*, 3(1):19–26, jan 2013. doi: 10.1515/green-2012-0028.
- [18] A T Elsayed, C R Lashway, and O A Mohammed. Advanced Battery Management and Diagnostic System for Smart Grid Infrastructure, 2016.
- [19] Ajay Raghavan, Peter Kiesel, Lars Wilko Sommer, Julian Schwartz, Alexander Lochbaum, Alex Hegyi, Andreas Schuh, Kyle Arakaki, Bhaskar Saha, Anurag Ganguli, Kyung Ho Kim, ChaeAh Kim, Hoe Jin Hah, SeokKoo Kim, Gyu-Ok Hwang, Geun-Chang Chung, Bokkyu Choi, and Mohamed Alamgir. Embedded fiber-optic sensing for accurate internal monitoring of cell state in advanced battery management systems part 1: Cell embedding method and performance. *Journal of Power Sources*, 341:466–473, feb 2017. doi: 10.1016/j.jpowsour.2016.11.104.
- [20] C.-F. Chiasserini and R.R. Rao. Energy efficient battery management. *IEEE Journal on Selected Areas in Communications*, 19(7):1235–1245, jul 2001. doi: 10.1109/49.932692.

-
- [21] Malin Andersson, Moritz Streb, Jing Ying Ko, Verena Löfqvist Klass, Matilda Klett, Henrik Ekström, Mikael Johansson, and Göran Lindbergh. Parametrization of physics-based battery models from input–output data: A review of methodology and current research. *Journal of Power Sources*, 521 (September 2021):230859, 2022. doi: 10.1016/j.jpowsour.2021.230859.
- [22] Venkat R. Subramanian, Vijayasekaran Boovaragavan, and Vinten D. Diwakar. Toward real-time simulation of physics based lithium-ion battery models. *Electrochemical and Solid-State Letters*, 10(11):255–260, 2007. doi: 10.1149/1.2776128.
- [23] L. Xia, E. Najafi, H.J. Bergveld, and M.C.F. Donkers. A Computationally Efficient Implementation of an Electrochemistry-Based Model for Lithium-Ion Batteries * *This work has received financial support from the Horizon 2020 programme of the European Union under the grant ‘Integrated Components for Complexity. *IFAC-PapersOnLine*, 50(1):2169–2174, jul 2017. doi: 10.1016/j.ifacol.2017.08.276.
- [24] D Grazioli, M Magri, and A Salvadori. Computational modeling of Li-ion batteries. *Computational Mechanics*, 58(6):889–909, dec 2016. doi: 10.1007/s00466-016-1325-8.
- [25] Woosuk Sung and Chee Burm Shin. Electrochemical model of a lithium-ion battery implemented into an automotive battery management system. *Computers and Chemical Engineering*, 76:87–97, 2015. doi: 10.1016/j.compchemeng.2015.02.007.
- [26] W Sung, D S Hwang, B.-J. Jeong, J Lee, and T Kwon. Electrochemical battery model and its parameter estimator for use in a battery management system of plug-in hybrid electric vehicles. *International Journal of Automotive Technology*, 17(3):493–508, jun 2016. doi: 10.1007/s12239-016-0051-8.
- [27] Michelle A. Kehs, Michael D. Beeney, and Hosam K. Fathy. Computational efficiency of solving the DFN battery model using descriptor form with Legendre polynomials and Galerkin projections. *Proceedings of the American Control Conference*, pages 260–267, 2014. doi: 10.1109/ACC.2014.6858858.
- [28] Xiaosong Hu, Shengbo Li, and Huei Peng. A comparative study of equivalent circuit models for Li-ion batteries. *Journal of Power Sources*, 198:359–367, jan 2012. doi: 10.1016/j.jpowsour.2011.10.013.
- [29] Joaquín Klee Barillas, Jiahao Li, Clemens Günther, and Michael A. Danzer. A comparative study and validation of state estimation algorithms for Li-ion

-
- batteries in battery management systems. *Applied Energy*, 155:455–462, 2015. doi: 10.1016/j.apenergy.2015.05.102.
- [30] Jiani Du, Zhitao Liu, and Youyi Wang. State of charge estimation for Li-ion battery based on model from extreme learning machine. *Control Engineering Practice*, 26:11–19, may 2014. doi: 10.1016/j.conengprac.2013.12.014.
- [31] Suresh Daravath, Edmund Burke, Paul Weist, and Huitian Lu. Lithium-Ion Battery Modelling and Online Battery Management Systems. In Coperich et al. K., editor, *Industrial and Systems Engineering Conference*, pages 1800–1806, Pittsburgh, Pennsylvania, USA, 2017. Institute of Industrial and Systems Engineers (IISE).
- [32] J.N. Hu, J.J. Hu, H.B. Lin, X.P. Li, C.L. Jiang, X.H. Qiu, and W.S. Li. State-of-charge estimation for battery management system using optimized support vector machine for regression. *Journal of Power Sources*, 269:682–693, 2014. doi: 10.1016/j.jpowsour.2014.07.016.
- [33] Doris L. Britton, Thomas B. Miller, and William R. Bennett. Thermal Characterization Study of Lithium-Ion Cells. In NASA Glenn Research Center, editor, *10th Electrochemical Power Sources Symposium*, page 26, Williamsburg, VA. United States, 2007. 10th Electrochemical Power Sources Symposium.
- [34] Carlos Adrian Correa-Florez, Andrea Michiorri, and George Kariniotakis. Optimal Participation of Residential Aggregators in Energy and Local Flexibility Markets. *IEEE Transactions on Smart Grid*, 11(2):1644–1656, mar 2020. doi: 10.1109/TSG.2019.2941687.
- [35] Matteo Boaro, Danilo Fuselli, Francesco De Angelis, Derong Liu, Qinglai Wei, and Francesco Piazza. Adaptive Dynamic Programming Algorithm for Renewable Energy Scheduling and Battery Management. *Cognitive Computation*, 5(2):264–277, 2013. doi: 10.1007/s12559-012-9191-y.
- [36] Carlos Adrian Correa-Florez, Alexis Gerossier, Andrea Michiorri, and Georges Kariniotakis. Stochastic operation of home energy management systems including battery cycling. *Applied Energy*, 225:1205–1218, sep 2018. doi: 10.1016/j.apenergy.2018.04.130.
- [37] Björn Weißhar and Wolfgang G Bessler. Model-based lifetime prediction of an LFP/graphite lithium-ion battery in a stationary photovoltaic battery system. *Journal of Energy Storage*, 14:179–191, dec 2017. doi: 10.1016/j.est.2017.10.002.

-
- [38] Eiko Kruger. *Développement d'algorithmes de gestion optimale des systèmes de stockage énergétique basés sur des modèles adaptatifs*. Theses, Université Grenoble Alpes, nov 2016.
- [39] Yuqing Yang, Stephen Bremner, Chris Menictas, and Merlinde Kay. Modelling and optimal energy management for battery energy storage systems in renewable energy systems: A review. *Renewable and Sustainable Energy Reviews*, 167(June):112671, 2022. doi: 10.1016/j.rser.2022.112671.
- [40] Jonathan Dumas, Colin Cointe, Antoine Wehenkel, Antonio Sutera, Xavier Fettweis, and Bertrand Cornelusse. A Probabilistic Forecast-Driven Strategy for a Risk-Aware Participation in the Capacity Firming Market. *IEEE Transactions on Sustainable Energy*, 13(2):1234–1243, apr 2022. doi: 10.1109/TSTE.2021.3117594.
- [41] Antonios Marinopoulos and Panagiotis Bakas. Evaluation of a very large scale PV power system with energy storage for capacity firming. In *2015 IEEE Eindhoven PowerTech*, pages 1–6. IEEE, jun 2015. doi: 10.1109/PTC.2015.7232761.
- [42] Jonathan Dumas, Bertrand Cornelusse, Antonello Giannitrapani, Simone Paoletti, and Antonio Vicino. Stochastic and deterministic formulations for capacity firming nominations. In *2020 International Conference on Probabilistic Methods Applied to Power Systems (PMAPS)*, pages 1–7. IEEE, aug 2020. doi: 10.1109/PMAPS47429.2020.9183646.
- [43] Sherif Abdelrazek and Sukumar Kamalasadan. A Weather-Based Optimal Storage Management Algorithm for PV Capacity Firming. *IEEE Transactions on Industry Applications*, 52(6):5175–5184, 2016. doi: 10.1109/TIA.2016.2598139.
- [44] Sunspec Alliance. Information Model Specification, 2015.
- [45] Sunspec Alliance. SunSpec Energy Storage Model, 2016.
- [46] Nicolas Damay, Christophe Forgez, Marie-pierre Bichat, Guy Friedrich, and Alejandro Ospina. Thermal modeling and experimental validation of a large prismatic Li-ion battery. In *IECON 2013 - 39th Annual Conference of the IEEE Industrial Electronics Society*, pages 4694–4699. IEEE, nov 2013. doi: 10.1109/IECON.2013.6699893.

-
- [47] Eric Prada. *Aging modeling and lifetime optimization of Li-ion LiFePO₄-graphite batteries according to the vehicle use*. Theses, Université Pierre et Marie Curie, nov 2012.
- [48] M.C. Smart, B.V. Ratnakumar, J. Whitacre, L. Whitcanack, K. Chin, M Rodriguez, and S. Surampudi. The effect of high temperature exposure upon the performance of lithium ion cells. In *Seventeenth Annual Battery Conference on Applications and Advances. Proceedings of Conference (Cat. No.02TH8576)*, pages 53–58. IEEE, 2002. doi: 10.1109/BCAA.2002.986368.
- [49] YuHeng Jiang, YiFei Yu, JianQing Huang, WeiWei Cai, and James Marco. Li-ion battery temperature estimation based on recurrent neural networks. *Science China Technological Sciences*, 64(6):1335–1344, jun 2021. doi: 10.1007/s11431-020-1736-5.
- [50] Saurabh Saxena, S Raghu Raman, B Saritha, and Vinod John. A novel approach for electrical circuit modeling of Li-ion battery for predicting the steady-state and dynamic I–V characteristics. *Sādhanā*, 41(5):479–487, may 2016. doi: 10.1007/s12046-016-0486-7.
- [51] David Ansean, Manuela Gonzalez, Juan Carlos Viera, Victor Manuel Garcia, Juan Carlos Alvarez, and Cecilio Blanco. Electric Vehicle Li-Ion Battery Evaluation Based on Internal Resistance Analysis. In *2014 IEEE Vehicle Power and Propulsion Conference (VPPC)*, pages 1–6. IEEE, oct 2014. doi: 10.1109/VPPC.2014.7007058.
- [52] Ruifeng Zhang, Bizhong Xia, Baohua Li, Yongzhi Lai, Weiwei Zheng, Huawen Wang, Wei Wang, and Mingwang Wang. Study on the Characteristics of a High Capacity Nickel Manganese Cobalt Oxide (NMC) Lithium-Ion Battery—An Experimental Investigation. *Energies*, 11(9):2275, aug 2018. doi: 10.3390/en11092275.
- [53] Cunxue Wu, Rujian Fu, Zhongming Xu, and Yang Chen. Improved State of Charge Estimation for High Power Lithium Ion Batteries Considering Current Dependence of Internal Resistance. *Energies*, 10(10):1486, sep 2017. doi: 10.3390/en10101486.
- [54] Hiroaki YOSHIDA, Nobutaka IMAMURA, Takefumi INOUE, Koichi TAKEDA, and Hitoshi NAITO. Verification of Life Estimation Model for Space Lithium-Ion Cells. *Electrochemistry*, 78(5):482–488, 2010. doi: 10.5796/electrochemistry.78.482.

-
- [55] Bolun Xu, Alexandre Oudalov, Andreas Ulbig, Göran Andersson, and Daniel S. Kirschen. Modeling of lithium-ion battery degradation for cell life assessment. *IEEE Transactions on Smart Grid*, 9(2):1131–1140, 2018. doi: 10.1109/TSG.2016.2578950.
- [56] Andrea Michiorri, Georges Kariniotakis, and Fiona Foucault. An aggregator for distributed energy storage units under multiple constraints in the nice grid demonstrator. In *CIREC Workshop 2014 - Grid operation and congestion management*, number 0371, pages 11–12, 2014.
- [57] William E Hart, Carl D Laird, Jean-Paul Watson, David L Woodruff, Gabriel A Hackebeil, Bethany L Nicholson, and John D Sirola. *Pyomo — Optimization Modeling in Python*, volume 67 of *Springer Optimization and Its Applications*. Springer International Publishing, Cham, third edition, 2017. doi: 10.1007/978-3-319-58821-6.
- [58] William E Hart, Jean-Paul Watson, and David L Woodruff. Pyomo: modeling and solving mathematical programs in Python. *Mathematical Programming Computation*, 3(3):219–260, sep 2011. doi: 10.1007/s12532-011-0026-8.
- [59] Andreas Wächter and Lorenz T. Biegler. On the implementation of an interior-point filter line-search algorithm for large-scale nonlinear programming. *Mathematical Programming*, 106(1):25–57, mar 2006. doi: 10.1007/s10107-004-0559-y.
- [60] M. Berecibar, I. Gandiaga, I. Villarreal, N. Omar, J. Van Mierlo, and P. Van Den Bossche. Critical review of state of health estimation methods of Li-ion batteries for real applications. *Renewable and Sustainable Energy Reviews*, 56:572–587, 2016. doi: 10.1016/j.rser.2015.11.042.
- [61] Rui Xiong, Jiayi Cao, Quanqing Yu, Hongwen He, and Fengchun Sun. Critical Review on the Battery State of Charge Estimation Methods for Electric Vehicles. *IEEE Access*, 6:1832–1843, 2017. doi: 10.1109/ACCESS.2017.2780258.
- [62] Dickson N T How, M A Hannan, and Senior Member. State of Charge Estimation for Lithium-Ion Batteries Using Model-Based and Data-Driven Methods : A Review. *IEEE Access*, 7:136116–136136, 2019. doi: 10.1109/ACCESS.2019.2942213.
- [63] Sijia Yang, Caiping Zhang, Jiuchun Jiang, Weige Zhang, Linjing Zhang, and Yubin Wang. Review on state-of-health of lithium-ion batteries: Characterizations, estimations and applications. *Journal of Cleaner Production*, 314 (June):128015, 2021. doi: 10.1016/j.jclepro.2021.128015.

-
- [64] John Wang, Ping Liu, Jocelyn Hicks-Garner, Elena Sherman, Souren Soukiazian, Mark Verbrugge, Harshad Tataria, James Musser, and Peter Finamore. Cycle-life model for graphite-lifepo4 cells. *Journal of Power Sources*, 196: 3942–3948, 2011. doi: 10.1016/j.jpowsour.2010.11.134.